Harmonic Resonance Stability Assessment in Aeronautical Ground Lighting Systems

D. Vidal, Ll. Monjo, L. Sainz

***Abstract*- Aeronautical ground lighting (AGL) systems assist aircraft pilots during airport operations. These systems are single-phase series circuits where constant current regulators feed luminaires with an adjustable rms current. These regulators are single-phase voltage source converters with PWM inverters based on insulated gate bipolar transistors to regulate the current. Constant current regulators may cause harmonic resonance instabilities when their control interacts with poorly damped resonances in the 0.75 – 2 kHz range. This paper studies these instabilities from the impedance-based representation of the AGL system. Approximated expressions of the constant current regulator and AGL circuit equivalent admittances are presented to assess system stability. A comprehensive overview of the influence that AGL system parameters have on harmonic resonance instabilities is presented and several recommendations on the AGL system components and constant current regulator parameters are proposed in order to improve system stability. Matlab/Simulink and PSCAD/EMTDC examples of a 68 luminaire AGL system are used to illustrate the contributions of this paper.**

***Index Terms*— AGL systems, harmonic resonance stability, impedance modeling, voltage source converters.**

I. Introduction

Aeronautical ground lighting (AGL) systems provide visual information during approach, landing and taxiing [1]. These systems are 1 to 10 km single-phase series circuits where constant current regulators (CCRs) feed luminaires through transformers with voltages up to 5 kV [1]–[4]. CCRs are single-phase voltage source converters (VSCs) with a typical current rating of 6.6 A which provide an adjustable rms current according to luminaire brightness requirements [4], [5]. Luminaires are visual references for pilots and their number ranges from 10 up to 300 in small and large AGL systems, respectively. These luminaires are usually halogen lamps but they are currently replaced by LED lamps due to energy saving policies. AGL transformers ensure series circuit continuity even in case of luminaire failure and isolate luminaires from the high operating voltages of the CCR primary circuit [6].

Harmonic resonances (from 0.75 to 2 kHz) can arise in AGL systems mainly due to the capacitive cable characteristics and the inductive transformer characteristics. These resonances can be analyzed from the AGL system equivalent circuit and frequency scan simulations [7]. However, analytical expressions are much more effective in characterizing resonance frequencies as a function of system parameters. CCRs may cause instabilities when their control interacts with poorly damping resonances in the 0.75 – 2 kHz range. These harmonic resonance instabilities are reported in other grid-connected VSCs such as HVDC links [8], [9], wind power plants [10], ac traction systems [11] and single-phase applications [12], [13]. In AGL systems, the resistance value of halogen lamps may be enough to prevent these instabilities but they could arise with LED lamps due to their low power consumption.

Frequency domain methods can be used to analyze the influence of system and control parameters on AGL system stability. The Nyquist criterion is the most used frequency domain method to assess stability [14], [15]. Other frequency domain methods such as the positive-net-damping stability criterion are based on the impedance characterization of the system which allows considering the individual contribution that source and load subsystems have on system stability [16], [17]. This criterion states that the system is stable if the net damping of the system (i.e., the sum of the source and load resistances or conductances) is positive at resonances (i.e., the system is passive at resonances). In the literature, a number of active damping methods are presented to limit resonance instabilities. These damping methods propose control loop modifications based on the system passivity [18], [19] and the positive-net-damping criterion [20]. These modifications aim to reshape the VSC impedance (or admittance) in order to increase its resistance (or conductance) and damp resonances. A few works also explore the influence that the control parameter values have on the VSC impedance to improve the VSC damping with an adequate choice of their values [19], [21].

This paper studies the AGL system stability. It analyzes the factors which could lead to system instability and proposes several solutions based on the modification of the CCR control parameters and AGL circuit components to improve AGL system stability. The paper also provides simple expressions of the CCR and AGL circuit equivalent admittances to analytically assess stability. A Matlab/Simulink application in a 68 luminaire AGL system is used to illustrate this study. PSCAD/EMTDC simulations with the AGL equivalent circuit in [7] are also used to validate the results.

D. Vidal is with the A.A.S.A. Airport of Reus, Spain (e-mail: dvlombarte@aena.es), Ll. Monjo is with the Dep. of Industrial and Design System Eng., Univ. Jaume I, Av. de Vicent Sos Baynat, s/n, 12071 Castelló de la Plana, Spain (mail: lmonjo@uji.es), L. Sainz is with the Dep. of Electrical Engineering, UPC, Av. Diagonal 647, 08028 Barcelona, Spain (mail: sainz@ee.upc.edu).

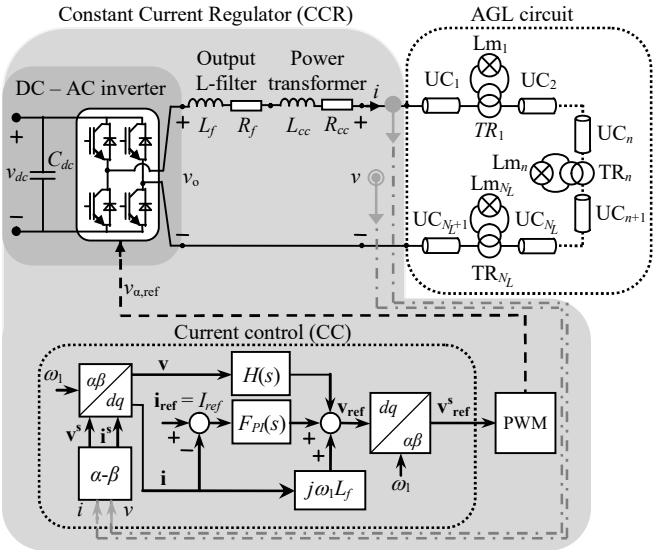

Fig. 1. AGL system (UC*n*: Underground cables. TR*n*: transformers. Lm*n*: Luminaires).

II. Impedance-Based Representation of Aeronautical Ground Lighting Systems

Harmonic resonances in the 0.75–2 kHz frequency range may cause instabilities in AGL systems due to the CCR negative-conductance response [8], [9]. Such instabilities, called as harmonic resonance instabilities, can be investigated in frequency-domain by using an impedance-based representation of AGL systems [14], [15], [18], [19]. This representation allows analyzing interactions between the harmonic resonances and the CCR negative-conductance response, studying the causes of harmonic resonance instabilities and proposing possible solutions.

Fig. 1 shows an AGL system with the AGL circuit and the CCR control block and circuit diagram. AGL systems are series circuits of copper insulated underground cables where CCRs supply N_L luminaires through transformers with adjustable rms current. The AGL transformers separate CCRs and luminaires into primary and secondary circuits, ensuring series circuit continuity and isolating luminaires from the primary circuit operating voltage, which can reach up to 5 kV [1]–[4]. CCRs adjust rms current to a reference current value I_{ref} according to luminaire brightness requirements but they may cause instabilities when their control interacts with poorly damped resonances. The impedance-based characterization of CCRs and AGL circuits is commonly used for assessing stability problems.

A. CCR modeling

The DC-AC inverter of CCRs receives the DC supply voltage v_{dc} from an AC-DC rectifier and provides an adjustable rms current according to AGL system requirements [1], [2], [4], [5], [12]. CCRs commonly use pulse width modulated (PWM) inverters based on insulated gate bipolar transistors (IGBTs) to regulate current, [5], and also include an output L-filter to reduce CCR current ripple and a power transformer to increase the output voltage and isolate CCRs from the AGL series circuit. CCRs are also usually fitted with earth fault detectors and lighting arrestors installed at their output terminals and output capacitors to mitigate high order harmonics of the PWM carrier frequency [5], [7]. These components are not included in Fig. 1 because they do not significantly affect the harmonic resonance stability assessment. The CCR control circuit provides the IGBTs with 5 – 8 kHz PWM trigger signals and adjusts their duty cycle based on the typical *dq* frame PI control [12], [13]. A feedback transformer coupled to the secondary winding of the CCR power transformer provides the voltage v and current i feedback signals to the PI controller. The *dq*-frame PI-based current control of CCRs is explicitly illustrated in Fig. 1 with bold letters denoting the complex space vectors (i.e., $\mathbf{x} = x_d + j \cdot x_q$). These space vectors are derived from the orthogonal transformation of the AGL components $x = v, i$ to the $\alpha\beta$-frame components $\mathbf{x^s} = x_\alpha + j \cdot x_\beta$ [13], and the subsequent transformation by means of transfer matrices determined at the AGL angular fundamental frequency $\omega_1 = 2\pi \cdot f_1$ ($f_1 = 50$ Hz) [18], [19].

Considering the *dq*-frame, the CCR model is obtained from the current dynamics at the output filter and power transformer terminals,

$$\mathbf{v_o} = (R + Ls + jL\omega_1)\mathbf{i} + \mathbf{v}, \tag{1}$$

and the CC voltage reference,

$$\mathbf{v_{ref}} = F_{\mathrm{PI}}(s)\left(\mathbf{i_{ref}} - \mathbf{i}\right) + jL\omega_1\mathbf{i} + H(s)\mathbf{v}, \tag{2}$$

where $\mathbf{v}$ and $\mathbf{i}$ are the AGL voltage and current, $\mathbf{v_o}$ is the DC-AC inverter output voltage, $\mathbf{i_{ref}} = I_{ref} + j \cdot 0$ is the CCR reference current, $R = R_f + R_{cc}$ and $L = L_f + L_{cc}$. The transfer functions of the PI controller and the AGL voltage feedforward low-pass filter are considered in the control as

$$F_{\mathrm{PI}}(s) = k_p + \frac{k_i}{s} \qquad H(s) = \frac{\alpha_f}{s + \alpha_f}, \tag{3}$$

where k_p and k_i are the PI control proportional and integral gains and $\alpha_f = 2\pi f_f$ is the low-pass filter bandwidth. The control design results in $k_p = \alpha_c L$ and $k_i = \alpha_c R$ where α_c is the current control bandwidth which should verify $\alpha_c \le 0.2 \cdot (2\pi f_{sw})$ with f_{sw} being the inverter switching frequency [18], [19]. The recommended low-pass filter bandwidth to ensure steady inverter current output is $\alpha_f \le 0.1\,\alpha_c$ [9], [21].

The DC-AC inverter output voltage $\mathbf{v_o}$ is related to the CCR voltage reference $\mathbf{v_{ref}}$ from the transfer function of the computation and switching process time delay T_d as follows [18], [19]:

$$\mathbf{v_o} = D(s)\mathbf{v_{ref}} \qquad D(s) = e^{-sT_d}. \tag{4}$$

This time delay is approximately given by $T_d \approx 1.5T_s$ with $T_s = 1/f_s$ and f_s being the inverter sampling frequency which, considering double-update PWM technique, is assumed twice the inverter switching frequency (i.e., $f_s = 2f_{sw}$) [9], [18].

The relation between the AGL voltage v and current i is

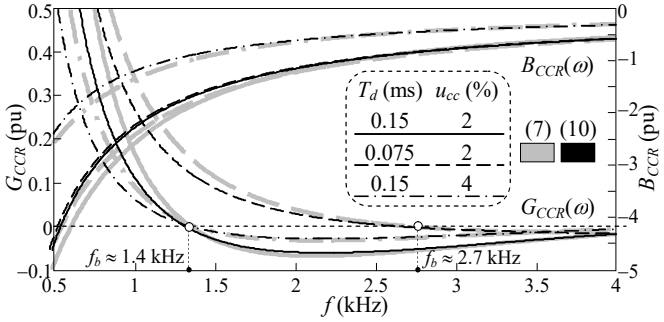

Fig. 2. Real and imaginary part of the CCR admittance ($G_{CCR}(\omega)$ and $B_{CCR}(\omega)$, respectively).

obtained from (1), (2) and (4) as

$$\mathbf{i} = F_{CCR}(s)\mathbf{i_{ref}} - Y_{CCR}(s)\mathbf{v}, \tag{5}$$

where $F_{CCR}(s)$ is the CCR closed-loop transfer function and $Y_{CCR}(s)$ is the CCR admittance,

$$\begin{aligned} F_{CCR}(s) &= \frac{D(s)F_{\mathrm{PI}}(s)}{R + Ls + jL\omega_1 + D(s)(F_{\mathrm{PI}}(s) - jL\omega_1)} \\ Y_{CCR}(s) &= \frac{1 - D(s)H(s)}{R + Ls + jL\omega_1 + D(s)(F_{\mathrm{PI}}(s) - jL\omega_1)}. \end{aligned} \tag{6}$$

The CCR admittance is expressed in frequency domain by setting $s = j\omega$ in (6) [15], [19],

$$Y_{CCR}(j\omega) = \frac{1 - D(j\omega)H(j\omega)}{R + jL(\omega + \omega_1) + D(j\omega)(F_{\mathrm{PI}}(j\omega) - jL\omega_1)}, \tag{7}$$

where $F_{\mathrm{PI}}(j\omega)$, $H(j\omega)$ and $D(j\omega)$ are written from (3) and (4) as

$$\begin{aligned} F_{\mathrm{PI}}(j\omega) &= k_p - j\frac{k_i}{\omega} \qquad H(j\omega) = \frac{\alpha_f}{\alpha_f + j\omega} \\ D(j\omega) &= \cos(\omega T_d) - j\sin(\omega T_d). \end{aligned} \tag{8}$$

The frequency response of the CCR admittance can be easily determined from (7) by using current software tools. However, an approximated expression of this admittance can be used to understand the influence that the CCR parameters have on AGL system stability. The CCR admittance in (7) can be simplified if the resistance R and the PI control integral gain k_i are neglected and $\omega >> \{\omega_1, \alpha_f\}$ is assumed at harmonic resonance frequencies [19],

$$Y_{CCR}(j\omega) \approx \frac{1}{k_p \cos(\omega T_d) - L\omega_1 \sin(\omega T_d) + jL\omega}, \tag{9}$$

Assuming that $k_p\cos(\omega T_d) - L\omega_1\sin(\omega T_d) << L\omega$ at harmonic resonances for the usual values of the CCR parameters, (9) can be simplified as

$$Y_{CCR}(j\omega) \approx \frac{k_p \cos(\omega T_d) - L\omega_1 \sin(\omega T_d)}{(L\omega)^2} - j\frac{1}{L\omega}. \tag{10}$$

Considering the data of the 25 kVA CCR in Table I (see Appendix), Fig. 2 compares the conductance $G_{CCR}(\omega) = \mathrm{Re}\{Y_{CCR}(j\omega)\}$ and the susceptance $B_{CCR}(\omega) = \mathrm{Im}\{Y_{CCR}(j\omega)\}$ of the CCR admittances in (7) and (10) for different values of T_d and u_{cc}. These conductance and susceptance are expressed in in per unit values, i.e. $Y_{CCR}(s)$ is multiplied by U_{N1}^2/S_N where S_N, U_{N1} are the rated power and primary voltage of the CCR power transformer. It is observed the reasonable accuracy of the approximated admittance (10) at frequencies of harmonic resonances. Moreover, the following comments can also be derived from (10) and Fig. 2,

- The CCR negative-conductance region is characterized from the boundary frequency f_b, which can be analytically obtained by solving the positive root of $G_{CCR}(\omega_b) = 0$,

$$\begin{aligned} & L\alpha_c \cos(\omega_b T_d) - L\omega_1 \sin(\omega_b T_d) = 0 \\ \Rightarrow \quad & f_b = \frac{\omega_b}{2\pi} = \frac{1}{2\pi}\frac{1}{T_d}\tan^{-1}(\alpha_c/\omega_1). \end{aligned} \tag{11}$$

- According to (11), the boundary frequency can be shifted to high frequencies by reducing the time delay T_d, i.e. by reducing the control computation time [9] and increasing the switching frequency.
- Considering that $k_p = L\alpha_c$, the CCR conductance value is reduced by increasing the L-filter and power transformer inductances because it is inversely proportional to these inductances (e.g., by increasing the short-circuit voltage u_{cc} of the CCR power transformer).

B. AGL circuit modeling

Fig. 3 shows the equivalent circuit of AGL circuits where underground cables, transformers and luminaires are replaced

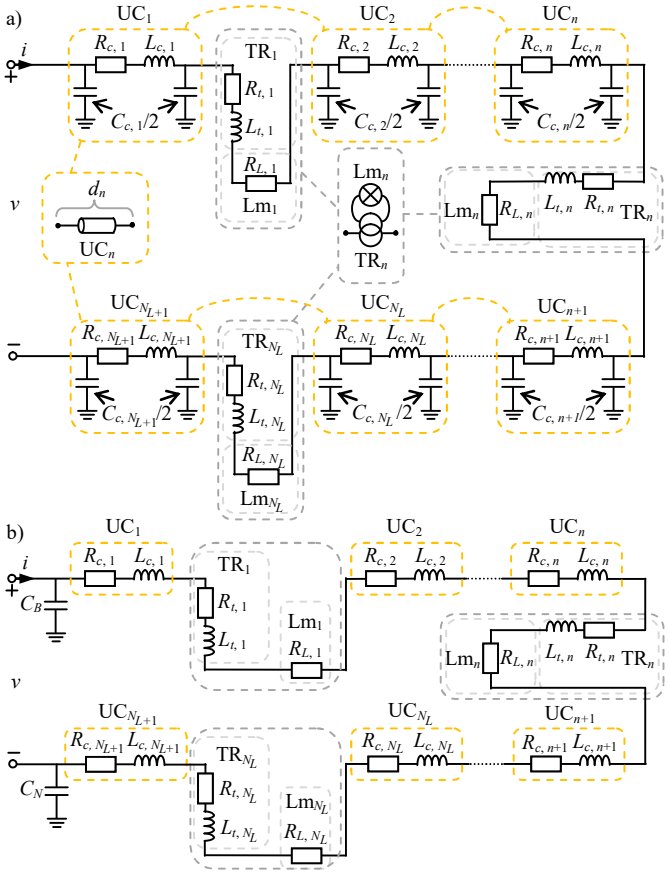

Fig. 3. AGL circuit (UC$_n$: Underground cables. TR$_n$: transformers. Lm$_n$: Luminaires): (a) Equivalent circuit. (b) Approximated equivalent circuit.

by their corresponding models.

AGL underground cables are modeled with a π-equivalent circuit based on concentrated parameter model [7]. The cable conductance is neglected and the concentrated parameters $R_{c,n}$, $L_{c,n}$ and $C_{c,n}$ are obtained from the distributed parameters R_x, L_x and C_x and length $d_{c,n}$ of the cable ($n = 1$ to N_{L+1}),

$$R_{c,n} = R_x \cdot d_{c,n} \qquad L_{c,n} = L_x \cdot d_{c,n} \qquad C_{c,n} = C_x \cdot d_{c,n}. \quad (12)$$

AGL transformers are single-phase transformers generally consisting of a rectangular magnetic core and separate primary and secondary windings [6]. Their power rating ranges from 30 to 500 W and their current ratio is generally 6.6/6.6 A. AGL transformers are characterized with the model proposed in [6] where $R_{t,n}$ and $L_{t,n}$ ($n = 1$ to N_L) are the winding resistance and leakage inductance and the core parameters are neglected in front of the luminaire impedance.

AGL luminaires are usually halogen lamps which are modelled as a resistance $R_{L,n}$. This resistance is accurately calculated from the luminaire active power $P_{L,n}$ and the current rating of the AGL system highest brightness step, i.e., $R_{L,n} = P_{L,n}/6.6^2$ ($n = 1$ to N_L) [7]. Nowadays, halogen lamps are being replaced by LED lamps in AGL systems due to energy saving policies. LED lamps are low consumption electronic non-linear loads which reduce AGL power consumption. However, system power quality may get worse and AGL system dynamics may also be affected due to the low power consumption and electronic characteristics of LED lamps. These lamps commonly have an active filtering circuit to correct the power factor and they could therefore be modeled as resistances whose value is calculated as halogen lamp resistance value. AGL transformers, and occasionally CCRs, may also be changed when the halogen lamps are replaced by LED lamps in order to adapt the transformer and CCR rated power to the LED lamp consumption.

The AGL circuit admittance $Y_{CIR}(s)$ can be determined by applying the node voltage method (NVM) to the AGL equivalent circuit in Fig. 3(a). However, the approximated equivalent circuit in Fig. 3(b) can be used to obtain a friendly expression of this admittance which allows understanding the influence that the AGL circuit parameters have on AGL system stability. In this approximation, the first half of the cable capacitors are grouped at the beginning of the circuit as C_B and the second half are grouped at the end as C_N, i.e.,

$$C_B = C_x \sum_{n=1}^{N_L/2} d_{c,n} \qquad C_N = C_x \sum_{n=N_L/2+1}^{N_L+1} d_{c,n}. \quad (13)$$

According to Fig. 3(b), the AGL circuit admittance is approximated as

$$Y_{CIR}(s) \approx C_E s + \frac{1}{R_E + L_E s}$$
$$C_E = \frac{C_B C_N}{C_B + C_N} \qquad R_E = R_{UC} + R_{TI} + R_{Lm} \qquad L_E = L_{UC} + L_{TI}, \quad (14)$$

where R_{UC}, R_{TI}, R_{Lm} are the total resistance of the AGL underground cables, transformers and luminaires, and L_{UC}, L_{TI} are the total inductances. i.e.

$$R_{UC} = \sum_{n=1}^{N_L+1} R_{c,n} = d_c R_x \qquad L_{UC} = \sum_{n=1}^{N_L+1} L_{c,n} = d_c L_x$$
$$R_{TR} = \sum_{n=1}^{N_L} R_{t,n} \qquad L_{TR} = \sum_{n=1}^{N_L} L_{t,n} \qquad R_{Lm} = \sum_{n=1}^{N_L} R_{L,n}, \quad (15)$$

and d_c is the total length of the AGL circuit,

$$d_c = \sum_{n=1}^{N_L+1} d_{c,n}. \quad (16)$$

The AGL circuit admittance is expressed in frequency domain by setting $s = j\omega$ in (14),

$$Y_{CIR}(j\omega) \approx \frac{R_E}{R_E^2 + (L_E\omega)^2} + j\left(C_E\omega - \frac{L_E\omega}{R_E^2 + (L_E\omega)^2}\right). \quad (17)$$

and, assuming that $R_E << L_E\omega$ at harmonic resonances for the usual values of the AGL circuit parameters, (17) can be simplified as

$$Y_{CIR}(j\omega) \approx \frac{R_E}{(L_E\omega)^2} + j\left(C_E\omega - \frac{1}{L_E\omega}\right). \quad (18)$$

Considering the data of the 68 luminaire AGL system in Table II (see Appendix), Fig. 4 compares the conductance $G_{CIR}(\omega) = \mathrm{Im}\{Y_{CIR}(j\omega)\}$ and the susceptance $B_{CIR}(\omega) = \mathrm{Re}\{Y_{CIR}(j\omega)\}$ of the AGL circuit admittance obtained from the NVM and (18) for different values of $P_{L,n}$ and $L_{t,n}$. These conductance and susceptance are expressed in in per unit values, i.e. $Y_{CIR}(s)$ is multiplied by U_{N2}^2/S_N where S_N, U_{N2} are the rated power and secondary voltage of the CCR power transformer. It is observed the reasonable accuracy of the approximated admittance (18) at frequencies of harmonic resonances. Moreover, the following comments can also be derived from (18) and Fig. 4,

- The value of the AGL circuit conductance is increased by increasing the luminaire power consumption (i.e., the luminaire resistances) and by decreasing the AGL cable and transformer inductances because this conductance is proportional to the equivalent resistances and inversely to

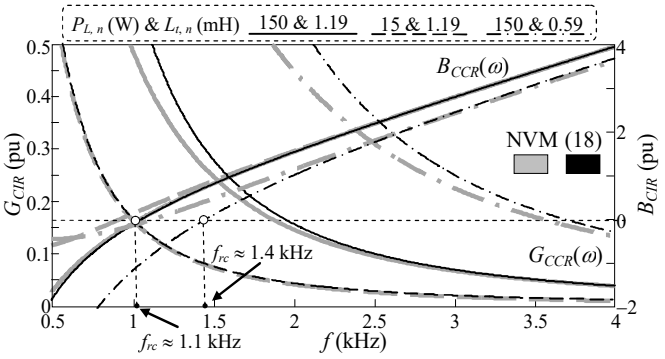

Fig. 4. Real and imaginary part of the AGL circuit admittance ($G_{CIR}(\omega)$ and $B_{CIR}(\omega)$, respectively).

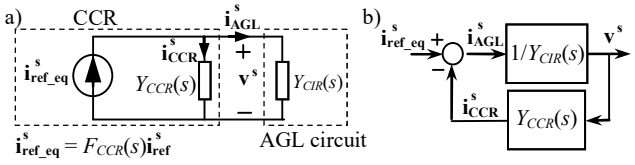

Fig. 5. AGL system modeling: a) Equivalent circuit. b) Closed-loop system.

the equivalent inductance square.

- High values of the AGL capacitors and inductances may shift parallel resonances to low frequencies according to $f_{rc} = 1/2\pi\sqrt{L_E C_E}$.

C. AGL system modeling

According to the previous CCR and AGL circuit models, the impedance-based equivalent circuit of AGL systems is shown in Fig. 5(a). The CCR is represented as a Norton equivalent source (5) and the AGL circuit is modeled with the equivalent admittance $Y_{CIR}(s)$ (14). It must be noted that the CCR (6) and AGL circuit (14) transfer functions are in *dq* and grid coordinates, respectively, and they must be in the same frame to assess stability. For that, these transfer functions are expressed in $\alpha\beta$ coordinates: the CCR closed-loop transfer function $F_{CCR}(s)$ and the equivalent admittance $Y_{CCR}(s)$ in (6) are transformed from *dq* coordinates to $\alpha\beta$ coordinates by means of the frequency translation $s \to s - \mathrm{j}\omega_1$ and the AGL circuit admittance $Y_{CIR}(s)$ in grid coordinates is the same as in $\alpha\beta$ coordinates [9], [19]. Moreover, the CCR and AGL circuit admittances are expressed in per unit values, i.e. $Y_{CCR}(s)$ is multiplied by U_{N1}^2/S_N and $Y_{CIR}(s)$ by U_{N2}^2/S_N where S_N, U_{N1} and U_{N2} are the rated power and voltages of the CCR power transformer.

The impedance-based equivalent circuit in Fig. 5(a) can also be represented as the closed-loop system in Fig. 5(b) considering the relation between the current source and the voltage at the CCR terminals,

$$\mathbf{v}^s = Z_t(s)F_{CCR}(s)\mathbf{i}^s_{ref} = \frac{1/Y_{CIR}(s)}{1+Y_{CCR}(s)/Y_{CIR}(s)}F_{CCR}(s)\mathbf{i}^s_{ref}, \quad (19)$$

which can be expressed by the following transfer functions

$$F(s) = Z_t(s) = \frac{M(s)}{1+L(s)} \qquad L(s) = M(s)N(s), \quad (20)$$

where $L(s)$ is the loop transfer function and $M(s) = 1/Y_{CIR}(s)$ and $N(s) = Y_{CCR}(s)$ are the open-loop and feedback transfer functions, respectively.

III. Stability Study of Aeronautical Ground Lighting Systems

The impedance-based equivalent circuit in Fig. 5(b) can be used to analyze stability considering the transfer function $F(s)$ of the closed-loop system representation (19).

A. AGL stability assessment

Frequency domain methods are commonly used to assess stability. The Nyquist criterion [14], [15] is a usual tool but it focuses on the loop transfer function $L(j\omega)$, which does not allow investigating separately the contribution of the CCR and the AGL circuit to the closed-loop stability. On the other hand, the positive-net-damping stability criterion avoids this drawback considering the stability contribution of each subsystem [16], [17], [20]. This criterion is derived from the Nyquist criterion and it relates the net damping and the harmonic resonances of the system with stability. Considering the frequency response of the CCR and the VSC admittances in Fig. 5 as follows:

$$Y_i(j\omega) = G_i(\omega) + jB_i(\omega) \qquad (i = CCR, CIR), \quad (21)$$

the positive-net-damping criterion states that the net damping $G(\omega) = G_{CCR}(\omega) + G_{CIR}(\omega)$ must be positive at harmonic frequencies of the system parallel resonances to ensure stability. Assuming that the resistive components of the CCR and AGL circuit can be neglected in comparison with the reactive components, these parallel resonances can be determined as

$$\mathrm{Im}\{Y_{CCR}(j\omega) + Y_{CIR}(j\omega)\} = B_{CCR}(\omega) + B_{CIR}(\omega) = 0, \quad (22)$$

which can also be analyzed from the impedance $Z_t(j\omega)$ in (19),

B. Comments and recommendations on AGL stability

AGL system stability can be easily analyzed from the positive-net-damping criterion. Considering the CCR and AGL circuit approximated expressions in (10) and (18), the harmonic frequency of the parallel resonance condition in $\alpha\beta$ frame is obtained as

$$B_{CCR}(\omega_r) + B_{CIR}(\omega_r) \approx -\frac{1}{L(\omega_r - \omega_1)} + C_E\omega_r - \frac{1}{L_E\omega_r} = 0$$
$$\Rightarrow \quad f_r = \frac{\omega_r}{2\pi} \approx \frac{1}{2\pi}\frac{1}{\sqrt{\frac{L\cdot L_E}{L+L_E}C_E}}, \quad (23)$$

and the net damping at harmonic resonance (23) is expressed from (10) and (18) as follows

$$G(\omega_r) = G_{CCR}(\omega_r) + G_{CIR}(\omega_r) \approx$$
$$\frac{\alpha_c\cos((\omega_r-\omega_1)T_d) - \omega_1\sin((\omega_r-\omega_1)T_d)}{L(\omega_r-\omega_1)^2} + \frac{R_E}{(L_E\omega_r)^2}. \quad (24)$$

It is observed that the damping of the AGL circuit $G_{CIR}(\omega)$ is positive for all frequencies and therefore, the net damping $G(\omega_r)$ will be only negative at f_r if the CCR damping $G_{CCR}(\omega_r)$ is negative and the damping contribution of the AGL circuit is smaller than the CCR damping contribution, i.e. if $G_{CCR}(\omega_r) < 0$ and $|G_{CCR}(\omega_r)| > |G_{CIR}(\omega_r)|$. The CCR damping $G_{CCR}(\omega_r)$ is negative if the frequency f_r is in the CCR negative-conductance region, i.e. if $f_r > f_b$ where f_b is the boundary frequency of this region (see Subsection II.A). The following comments on the AGL system stability can be derived from the above results:

- In general, the damping contribution of the halogen lamps in (14) (i.e., the resistance of halogen lamps $R_{L,n} = P_{L,n}/6.6^2$)

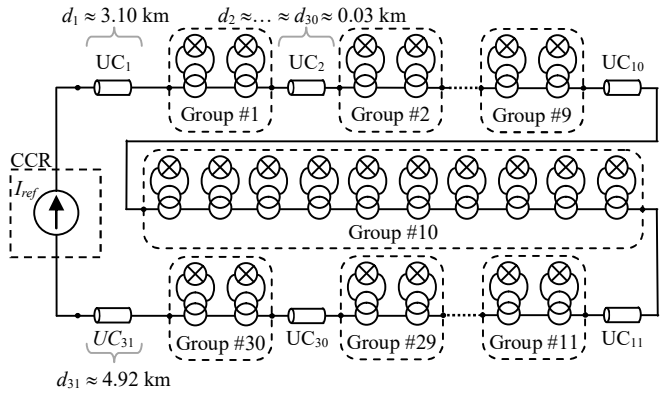

Fig. 6. 68 luminaire AGL system.

is enough to ensure AGL system stability, i.e., to ensure that $|G_{CCR}(\omega_r)| < |G_{CIR}(\omega_r)|$.

- The halogen lamps replacement with LED lamps reduce the AGL circuit damping $G_{CIR}(\omega)$ because the resistance of LED lamps is smaller, and this may cause the AGL system instability if $G_{CCR}(\omega_r) < 0$ and $|G_{CCR}(\omega_r)| > |G_{CIR}(\omega_r)|$.
- The possibility of harmonic resonance instabilities in small AGL systems is smaller than in large AGL systems because the total length of the AGL system is smaller and therefore the equivalent capacitor and inductor values of the underground cables are smaller shifting the harmonic resonance to high frequencies. The reduction of the inductor values also increases the contribution of the AGL circuit damping (18) improving system stability.

The following recommendations to improve AGL system stability can also be derived:

- Reduce the rated power of the AGL transformers and CCR according with the power consumption of LED lamps may decrease the inductance $L_{t,n}$ of the AGL transformers, which increases $G_{CIR}(\omega)$ and may also shift f_r far from the negative damping region.
- Reduce the computation time delay of the CCR and increase the switching frequency reduces the CCR time delay T_d and may shift f_b above the resonance frequencies.

IV. Application

Stability of the Reus airport (Catalunya, Spain) approach lightning system in Fig. 6 is analyzed [7]. This system has a 25 kVA CCR supplying 68 luminaires of 150 W connected through 150 W 6.6/6.6 A 50 Hz transformers along 8.89 km (see data in Appendix). The frequency response of the impedance $Z_t(j\omega) = (Y_{CCR}(j\omega) + Y_{CIR}(j\omega))^{-1}$ (19) and the dampings $G(\omega)$,$G_{CCR}(\omega)$ and $G_{CIR}(\omega)$ as well as the Nyquist plots of the loop transfer function $L(j\omega)$ and the PSCAD/EMTDC simulation plots of the CCR connection dynamics are shown in Fig. 7 to illustrate the 68 luminaire AGL system stability.

System stability with the halogen lamps in Table II (Case #1) and with LED lamps of 15 W (Case #2) is analyzed in Fig. 7(a) and (b), respectively. The stable response of the AGL system with halogen lamps (Case #1) is predicted with the positive-net-damping criterion in Fig. 7(a) because the parallel resonance at $f_r = 1.85$ kHz is in the positive-damping region of $G(\omega)$. It must be noted that, although f_r is greater than $f_b = 1.42$ kHz (i.e., $G_{CCR}(\omega) < 0$ at f_r), the contribution of the AGL circuit conductance lead to AGL system stability due to $|G_{CCR}(\omega_r)| < |G_{CIR}(\omega_r)|$. The Nyquist plot of the loop transfer function $L(j\omega)$ confirms this result because the Nyquist curve does not encircle the −1 (nor the open-loop system has positive poles). The halogen lamp replacement by 15 W LED lamps (Case #2) leads to an unstable response of the AGL system which is predicted with the positive-net-damping criterion in Fig. 7(b) because the parallel resonance at $f_r = 1.86$ kHz is in the negative-damping region of $G(\omega)$. In this case, it is observed that f_r is also greater than $f_b = 1.42$ kHz and the contribution of the AGL circuit conductance is not enough to obtain AGL system stability, i.e. $|G_{CCR}(\omega_r)| > |G_{CIR}(\omega_r)|$ due to the small LED lamp power consumption. The Nyquist plot of the loop transfer function confirms this result because the Nyquist curve intersects the unit circle at 1.86 kHz encircling the −1 point in clockwise direction. Time-domain simulations in PSCAD/EMTDC are shown in Fig. 7(a) and (b) when the CCR is connected. It is verified the stable and unstable response of the AGL system in Case #1 and #2, respectively.

Several measures on the AGL system components and CCR control parameters can be applied in order to achieve the stability of the 68 luminaire system with LED lamps. Regard to the AGL system components, Fig. 7(c) shows the stable response of the system when the 150 W AGL transformers are replaced by 45 W AGL transformers ($R_{t,n} = 0.187\ \Omega$ and $L_{t,n} = 0.37$ mH [6]) in order to adapt the transformer rated power to the LED lamp consumption (Case #3). It can be observed that the 45 W AGL transformer inductance $L_{t,n}$ is smaller than the 150 W AGL transformer inductance which increases the contribution of the AGL circuit conductance (see Subsection III.B) and $|G_{CIR}(\omega_r)|$ becomes greater than $|G_{CCR}(\omega_r)|$. This ensures that parallel resonance at $f_r = 2.33$ kHz is in the positive-damping region of $G(\omega)$. Note that the reduction of the AGL circuit inductance does not modify the boundary frequency f_b but increases the resonance frequency f_r (23). The stability results are confirmed by the Nyquist plot and the PSCAD/EMTDC simulations. AGL transformers of smaller rated power could be used which further improve stability. Also, the replacement of the 25 kVA CCR by a 2.5 kVA CCR with a 300/400 V power transformer may be made in order to obtain system stability (results are not shown for sake of space). Regard to the CCR control parameters, Fig. 7(d) and (e) show how the reduction of the control computation time delay, $T_d = T_s$, (Case #4) and the increasing of the switching frequency f_{sw} up to 8 kHz (Case #5) lead to a reduction of the CCR time delay T_d which increases the boundary frequency to $f_b = 2.11$ and 2.25 kHz, respectively. This boundary frequency becomes greater than the resonance frequency f_r and therefore it is verified that $G_{CCR}(\omega) > 0$ at f_r. Nyquist plot and PSCAD/EMTDC simulations validate this result.

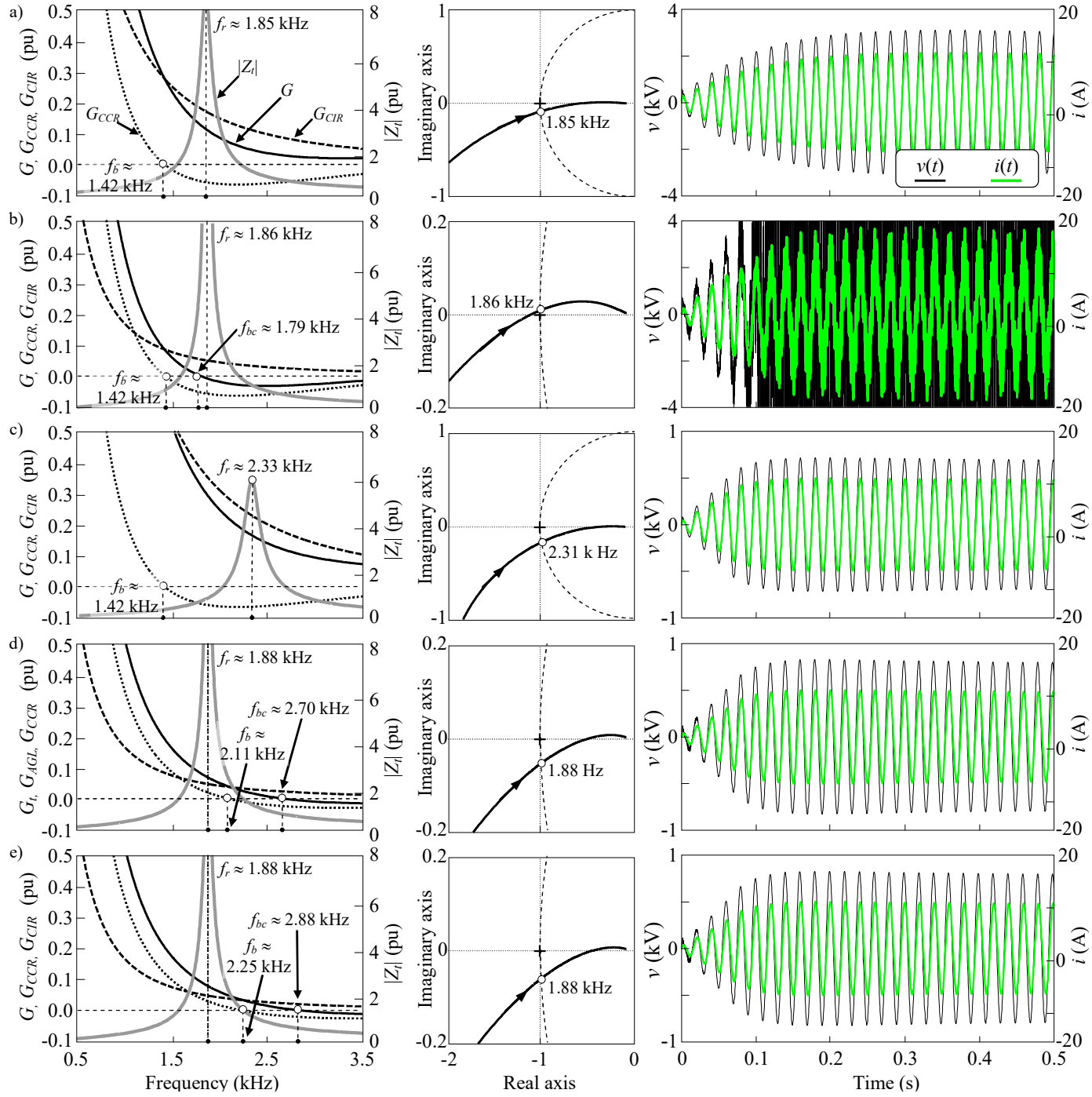

Fig. 7. Application results: a) Case #1. b) Case #2. c) Case #3. d) Case #4. e) Case #5.

Fig. 8 shows the frequency response of the impedance $Z_t(j\omega)$ and the net damping $G(\omega)$ for different number of LED luminaires in order to illustrate the stable response of small AGL systems. It can be observed that damping increases to positive values and resonance frequency shifts to high values in small AGL systems which favors system stability.

V. Conclusions

This paper analyzes AGL system stability. It is concluded that the damping of halogen lamps may be enough to prevent instabilities in AGL systems but these instabilities may arise in large AGL crcuits where halogen lamps are replaced by LED lamps. Simple expressions of the CCR and the AGL circuit admittances are presented in the paper to analyze the causes of instabilities and propose solutions. Several recommendations on the AGL system components and CCR control parameters are proposed in order to improve AGL system stability. The reduction of the AGL transformer and CCR rated power according with the LED lamp power consumption and the reduction of the CCR time delay may improve this stability.

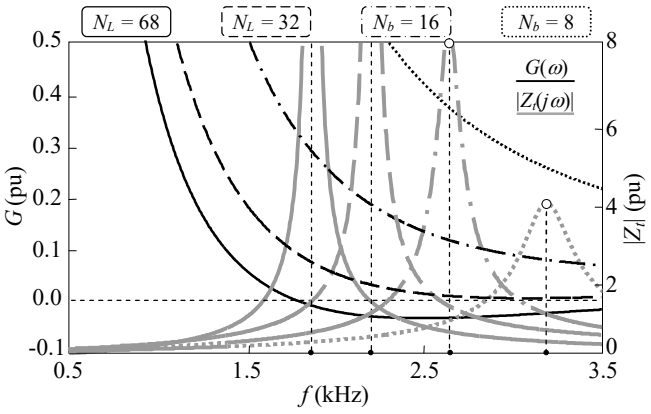

Fig. 8. Influence of AGL system size on stability.

APPENDIX: AGL SYSTEM DATA

The data of a 68 luminaire AGL system were obtained from the technical support of Aena Aeropuertos S.A Reus Airport (Spain). These data were used in several field measurement works conducted on AGL circuits at Reus airport (Catalunya, Spain) [6], [7]. The CCR and AGL circuit data are shown in Table I and Table II, respectively. The data were obtained from manufacturer datasheets and laboratory and field measurements. In particular, the AGL transformer data values were obtained from laboratory measurements [6].

REFERENCES

TABLE I
25 KVA CONSTANT CURRENT REGULATOR DATA (ω_1 =2π50 rad/s)

	Parameters	Values
CCR	S_N (kVA)	25
Power transformer	U_{N1}/U_{N2} (kV)	0.3/4
$Z_b = U_{N1}^2/S_N$	u_{cc} (%)	2
$L_{cc}\omega_1 = Z_b \cdot u_{cc}/100$	L_{cc} (mH)	0.023
$R_{cc}/(L_{cc}\omega_1) = 0.01$	R_{cc} (mΩ)	0.72
Output L-filter	L_f (mH)	0.02
	R_f (mΩ)	0.06
Current control	f_{sw} (kHz)	5
	$\tau_c = 1/\alpha_c$ (ms)	1
$k_p = \alpha_c(L_t + L_f)$	$\alpha_f = 0.1\,\alpha_c$ (rad/s)	100
$k_i = \alpha_c(R_t + R_f)$	$T_d = 0.75/f_{sw}$ (ms)	0.15

TABLE II
68 LUMINAIRE AGL CIRCUIT DATA [6], [7]

	Parameters	Values
Halogen lamp luminaires	P (W)	150
6.6/6.6 A, 50 Hz AGL transformers	P (W)	150
	R_t (Ω)	0.281
	L_t (mH)	1.19
Underground cables	R_x (Ω/km)	3.98
	L_x (mH/km)	0.547
	C_x (μF/km)	0.126

[1] Aerodrome design manual, Part 4: Visual aids, International Civil Aviation Organization, 2004 4th Edn.

[2] Aerodromes, Volume I: Aerodrome design and operations, Annex 14 to the convention on International Civili Aviation, International Civil Aviation Organization, 2004 4th Edn.

[3] N. Saraf, R. Salvi, N. Salunkhe and R. Sahasrabuddhe, "Airfield lamp monitoring & control systems," *Int. Conf. on Information, Communication and Embedded Systems (ICICES 2013)*, Febr. 2013, pp. 1141-1143.

[4] P. E., Kevin, "Integration of aviation lighting system and computer controlled monitoring system," *IEEE Int. Conf. on Systems, Man and Cybernetics*, Oct. 1996, 1132-1137.

[5] OCEM AirfieldTechnology, Constant current regulators. New generation, EnergyTechnology, Bologna, Italy, 2015.

[6] D. Vidal, Ll. Monjo, L. Sainz and J. Pedra, "Model of aeronautical ground lighting system transformer," *IET Electric Power Applications*, vol. 9, no. 3, pp. 239-247, March 2015.

[7] D. Vidal, Ll. Monjo, L. Sainz and J. Pedra, "Aeronautical ground lighting system study: field measurement and simulations," *IET Generation, Transmission and Distribution*, vol. 10, no. 13, pp. 3228-3233, Oct. 2016.

[8] C. Buchhagen, C. Rauscher and A. Menze, "BornWin1 – First experiences with harmonic interactions in converter dominated grids,"*Proc. of the International ETG Congress 2015*, Nov. 2015, pp. 27-33.

[9] L. Harnefors, X. Wang, A. G. Yepes and F. Blaabjerg, "Passivity-based stability assessment of grid-connected VSCs – An overview," *IEEE Journal of Emerging and Selected Topics in Power Electronics*, vol. 4, no. 1, pp. 116–125, March 2016.

[10] F. D. Freijedo, S. K. Chaudhary, R. Teodorescu, J. M. Guerrero, C. L. Bak, L. H. Kocewiak and C. F. Jensen, "Harmonic resonances in wind power plants: modeling, analysis and active mitigation methods," *Proc. of the IEEE PowerTech Eindhoven*, June-July 2015, pp. 1-6.

[11] E. Möllerstedt and B. Bernhardsson, "Out of control because of harmonics – An analysis of the harmonic response of an inverter locomotive," *IEEE Control Syst. Mag*., vol. 20, no. 4, pp. 70-81, Aug. 2000.

[12] T-F. Wu, L-C. Ning and Y.C. Chang, "Extended-application of D-Σ digital control to a single-phase bidirectional inverter with an LCL filter," *IEEE Trans. on Power Electronics*, vol. 30, no. 7, pp. 3903–3911, July 2015.

[13] T. Merabet, K. Tawfique, H. Ibrahim, R. Beguenane and A. Ghias, "Energy management and control system for laboratory scale microgrid based wind-PV-battery," *IEEE Trans. on Sustainable Energy*, vol. 8, no. 1, pp. 145–154, Jan. 2017.

[14] J. Sun, "Impedance-based stability criterion for grid-connected inverters," *IEEE Transactions on Power Electronics*, vol. 26, no. 11, pp. 3075–3078, Nov. 2011.

[15] M. Céspedes and J. Sun, "Impedance modelling and analysis of grid-connected voltage-source converters," *IEEE Trans. on Power Electronics*, vol. 29, no. 3, pp. 1254–1261, Nov. 2014.

[16] L. Harnefors, "Proof and application of the positive-net-damping stability criterion," *IEEE Trans. on Power Systems*, vol. 26, no. 1, pp. 481-482, Feb. 2011.

[17] L. Sainz, M. Cheah-Mane, Ll. Monjo, J. Liang and O. Gomis-Bellmunt, "Positive-net-damping stability criterion in grid-connected VSC systems," *IEEE Journal of Emerging and Selected Topics in Power Electronics*, Accepted for publication (DOI: 101109/JESTPE.2017.2707533).

[18] L. Harnefors, X. Wang, A. G. Yepes, and F. Blaabjerg, "Passivity-based stability assessment of grid-connected VSCs – An overview," *IEEE Journal of Emerging and Selected Topics in Power Electronics*, vol. 4, no. 1, pp. 116–125, March 2016.

[19] L. Harnefors, M. Bongiorno and S. Lundberg, "Input-admittance calculation and shaping for controlled voltage-source converters," *IEEE Trans. on Industrial Electronics*, vol. 54, no. 6, pp. 3323-3334, Dec. 2007.

[20] G. Stamatiou and M. Bongiorno, "Stability Analysis of Two-Terminal VSC-HVDC Systems using Net-Damping Criterion," *IEEE Trans. on Power Delivery*, vol. 31, no. 4, pp. 1748-1756, Aug. 2016.

[21] M. Zhao, X. Yuang, J. Hu. and Y. Yan, "Voltage dynamics of current control time-scale in a VSC-connected weak grid," *IEEE Transactions on Power Systems*, vol. 31, no. 4, pp. 2925-2937, July 2016.